

Ab Initio Study of Spectral and Thermochemical Properties of 1*H*-Phospholes

David Delaere, Nguyen-Nguyen Pham-Tran, and Minh Tho Nguyen*

Department of Chemistry, University of Leuven, Celestijnenlaan 200F, B-3001 Leuven, Belgium

Received: May 21, 2003; In Final Form: July 9, 2003

The purpose of this work is to (re)interpret some spectral and thermochemical properties of 1*H*-phospholes. The first topic covers the assignment of absorption bands in their photoelectron and UV–vis electronic spectra. Our goal is to unravel the electronic origin of the observed bands. The second topic deals with their basicity. We investigated the site of protonation and the basicity of 1*H*-phospholes in both the gas phase and acidic solution. To elucidate structure–property relationships, we studied in a systematic way the influence of common substituents on the electronic structure and emphasized the corresponding consequences for the spectral and thermochemical properties. The geometric and electronic structures were investigated using adequate quantum-chemical techniques including multiconfiguration SCF and density functional theory based methods.

Introduction

Phospholes form a class of compounds based on a fully unsaturated five-membered ring containing a phosphorus atom. Several recent and comprehensive reviews cover the rich chemistry of phospholes.^{1–5}

The 1*H*-phospholes are P-analogues of the better known pyrroles. For some time after their discovery, the key issue concerning phospholes was their potential aromaticity. Today, the debate is apparently over, and it is widely accepted that phospholes are nonaromatic. The stabilization of their planar state by electronic delocalization is substantial but not sufficient enough to overcome the intrinsically high inversion barrier of phosphorus. As a result, phospholes remain pyramidal in their ground state, albeit with a sharply reduced inversion barrier. Because of the poor overlap between the phosphorus lone pair and the *cis*-1,3-butadienic π -orbitals in their ground state, phospholes behave as a loose combination of a phosphine and a *cis*-1,3-butadiene unit and possess only a weak cyclic π -conjugation. As a consequence, they chemically resemble cyclopentadienes more than pyrroles. Despite the large wealth of available literature, many basic properties of simple phospholes are not well established.

The purpose of this work is therefore to (re)interpret some spectral and thermochemical properties of 1*H*-phospholes. The first topic covers the assignment of absorption bands in their PES and UV–vis spectra. Our goal is to unravel the electronic origin of the observed bands. The second topic deals with their basicity. We thus investigate the site of protonation and the basicity of 1*H*-phospholes in both gas phase and acidic solution. These spectral and thermochemical properties are closely related to the electronic structure, which is reliably described by adequate quantum-chemical techniques.

Different substituted 1*H*-phospholes, which are experimentally known, have been considered and are presented in Figure 1. The impact of substituent effects on the spectral and thermochemical properties was examined in a systematic way. We started analyzing the influence of methyl and phenyl

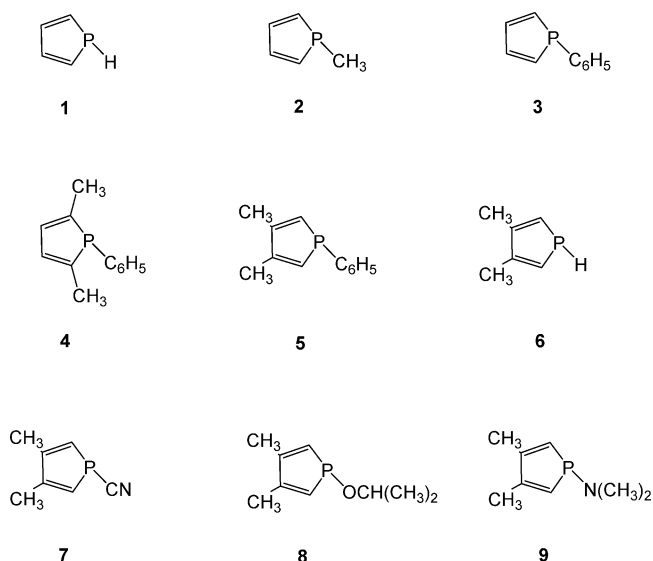


Figure 1. 1*H*-phospholes considered: phosphole (1), 1-methylphosphole (2), 1-phenylphosphole (3), 2,5-dimethyl-1-phenylphosphole (4), 3,4-dimethyl-1-phenylphosphole (5), 3,4-dimethylphosphole (6), 3,4-dimethyl-1-cyanophosphole (7), 3,4-dimethyl-1-isopropoxyphosphole (8), and 3,4-dimethyl-1-dimethylaminophosphole (9).

substitution at the P position of the five-membered ring. Subsequently, the influence of dimethyl substitution at 2,5- and 3,4-positions of 1-phenylphosphole was studied. Finally, we considered the influence of π -acceptor and π -donor substituents such as cyano and isopropoxy, dimethylamino groups, respectively, at the P position of 3,4-dimethylphospholes.

Computational Details

Ionization Energies. The Hartree–Fock (HF) method⁶ allows us to obtain approximate solutions of the electronic Schrödinger equation. Here, the calculated molecular orbital energies are related to the experimental *vertical ionization energies* by using Koopmans’ theorem. As such, HF wave functions can already be used for predicting and interpreting signals observed in a UV–PES spectrum. The *adiabatic ionization energy* corre-

* Corresponding author. Fax: 32-16-32 79 92. E-mail: minh.nguyen@chem.kuleuven.ac.be.

sponds to the lowest energy required to carry out the removal of an electron from a molecule, and is related to the transition from the lowest electronic, vibrational, and rotational level of the isolated molecule to the lowest electronic, vibrational, and rotational level of the isolated cation.

Geometrical parameters of all structures considered were optimized using the B3LYP functional of density functional theory in conjunction with the 6-31G(d) basis set. The *vertical ionization energies* were evaluated using HF/6-31G(d) wave functions, based on B3LYP/6-31G(d) optimized geometries. The *adiabatic ionization energies* were calculated at the B3LYP/6-31G(d) level using the ΔE procedure.⁷ Thereby, the structures of the ionic ground state and the neutral molecule were optimized separately.

Excited States. The accurate calculation of excited electronic states has long been a challenge for quantum chemistry. The possibility for accurate calculations of such states in molecules has only recently been made possible through the development of new quantum chemical techniques. The *complete active space multiconfigurational method followed by second-order perturbation theory* (CASPT2)⁸ is currently one of the more successful methods for treating excited states and the *multistate* option of it (MS-CASPT2)⁹ is capable of handling the valence–Rydberg mixing. However, the CASPT2 method has the basic limitation of the size and selection of the active space in the preliminary state average restricted active space (RASSCF) step. In this work, the valence excited singlet states of the parent phosphole (1) were investigated using both MS-CASPT2 and the time-dependent density functional theory (TD-DFT)^{10,11} methods. By way of comparison, we were able to evaluate the accuracy of the more economical TD-DFT method, which will then be applied to the larger substituted phospholes. All these calculations were performed at the MP2/6-311++G(d,p) optimized ground-state geometries.

Before a MS-CASPT2 calculation can be performed, a *state-average RASSCF* wave function should be available. Both types of calculations are briefly described below. We also emphasize the importance of the selection of proper active spaces and appropriate diffuse basis functions.

Basis Sets. Generally contracted basis sets of the atomic natural orbital (ANO) type^{12,13} were used. The contraction scheme employed was P[5s4p2d]/C[4s3p1d]/H[2s1p]. To be able to handle the valence–Rydberg mixing, the original basis sets were supplemented with a set of 1s1p1d diffuse functions. These functions were added at the charge centroid of the cation, as suggested by Dunning and Hay.¹⁴ As exponents for the diffuse functions we used those optimized by Kaufmann et al.¹⁵

State-Average RASSCF. The description of the ground-state electronic structure of phosphole suggests that at least the three π and two π^* valence orbitals need to be included in the active space. For the parent phosphole (1), which belongs to the C_s point group, this set corresponds to three a' and two a'' orbitals. However, the valence states are not the only states present at low energies. In a gas phase spectrum of a neutral molecule, the Rydberg states start to appear at energies above 5 eV. Therefore, excitations to the 3s, 3p, and 3d Rydberg orbitals must be simultaneously included in the calculations. The Rydberg orbitals can be classified into the point group as their corresponding atomic orbitals. Accordingly, for phosphole (1), the 3s, 3p_x, 3p_z, 3d_{x²-y²}, 3d_{z²} and 3d_{xz} orbitals belong to the irreducible representation a' , whereas the 3p_y, 3d_{xy} and 3d_{yz} orbitals belong to a'' . The active space used for computing the valence $\pi^* \leftarrow \pi$ states of phosphole thus comprises nine orbitals of symmetry a' and five orbitals of symmetry a'' . In the

resulting active space, we considered six active electrons. The reported valence $\pi^* \leftarrow \pi$ states belong to the A' and A'' symmetries. The RASSCF energies and wave functions were obtained from average energy calculations in each symmetry. In both A' and A'' symmetries, the molecular orbitals were determined by averaging over the 11 lowest states. A level shift parameter of 0.2 au was used. The multistate CASPT2 method⁹ is an extension of the multiconfigurational second-order perturbation approach CASPT2. It considers the coupling of a number of CASPT2 states of the same symmetry, which is a crucial condition to solve the erratic valence–Rydberg mixing. The treatment was performed on the same number of states as the averaging in the previously mentioned RASSCF calculation. For this purpose, a level shift parameter of 0.3 au was selected.

The excitation energies to the lowest valence excited singlet states, the corresponding oscillator strengths and expectation values for $\langle r^2 \rangle$ were also determined using *time-dependent DFT*.^{10,11} The computations were performed employing the B3LYP functional. The basis sets used were TZVP¹⁶ (triplet ζ valence plus polarization set) augmented with diffuse s and p functions on the phosphorus atom and SV(P) (split valence plus polarization set). TD-DFT is considered as a suitable method for the calculation of excitation energies of organic molecules whose ground state is well represented by a single configuration and for excited states dominated by a single orbital excitation from the ground state.¹⁷

The geometry optimizations have been carried out with the Gaussian 98¹⁸ program. The MS-CASPT2 calculations were performed with Molcas¹⁹ and the TD-DFT calculations with Turbomole.²⁰

Basicity. The *basicity* of phospholes in *gas phase* is measured by their proton affinity (PA), which is the negative of the enthalpy change of the reaction



where B and BH⁺ denote the base and its conjugate acid, respectively. Equation 2 was used to calculate the absolute proton affinity^{21–24}

$$PA = -\Delta H = \Delta E_{el} + \Delta ZPE + \frac{5}{2}RT \quad (2)$$

where ΔE_{el} represents the difference in electronic energies between the neutral and protonated forms at 0 K. ΔZPE corresponds to the difference in zero-point energies, whereas the last term, $\frac{5}{2}RT$, describes the thermodynamic temperature correction. The absolute proton affinities were calculated by means of *density functional theory* at B3LYP/6-311++G(d,p)//HF/6-31G(d,p) level. It is evident that the higher the proton affinity, the more basic the molecule.

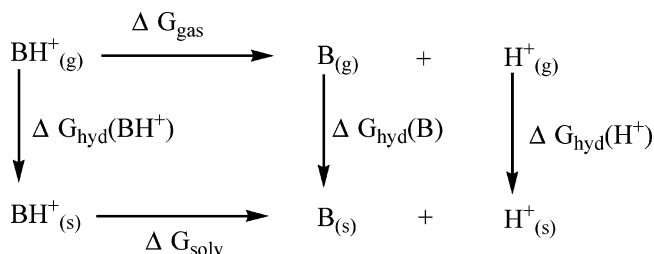
The most convenient way of measuring the *basicity* of phospholes in *acidic solution* is to look at the acidity (pK_a) of the corresponding phospholium ions. Since a more strongly basic phosphole holds a proton more tightly, its corresponding phospholium ion is less acidic (higher pK_a) and vice versa. The pK_a value is defined^{25,26} as

$$pK_a = -\log K_a$$

$$\Delta G^\circ = -2.3RT \times \log K_a$$

$$pK_a = \frac{\Delta G^\circ}{2.3RT} \quad (3)$$

The thermodynamic cycle relevant to the solvation processes is shown below:



It follows that the $\text{p}K_{\text{a}}$ value can be calculated from the Gibbs free energy of the reaction



whereby

$$\text{p}K_{\text{a}} = \frac{1}{2.3RT} [\Delta G_{\text{hyd}}(\text{B}) + \Delta G_{\text{hyd}}(\text{H}^+) - \Delta G_{\text{hyd}}(\text{BH}^+) + \Delta G_{\text{gas}}(\text{BH}^+)] \quad (5)$$

The gas-phase basicity for BH^+ is given by

$$\Delta G_{\text{gas}}(\text{BH}^+) = G_{\text{g}}(\text{B}) + G_{\text{g}}(\text{H}^+) - G_{\text{g}}(\text{BH}^+) \quad (6)$$

We notice that the experimental values for $G_{\text{gas}}(\text{H}^+)$ and $G_{\text{hyd}}(\text{H}^+)$ amount to -6.28 and -259.5 kcal/mol, respectively. The Gibbs free energy change of the reaction in gas phase, ΔG_{gas} , was computed at the same level of theory used for the gas phase proton affinity (B3LYP/6-311++G(d,p)//HF/6-31G(d,p)). The hydration Gibbs free energy difference, ΔG_{solv} , was calculated using the polarizable continuum solvation model (PCM),²⁷ in which the UAHF definition was used for the construction of the cavities. The computations for neutral and protonated forms in solvent were performed at the HF/6-31G(d,p) and HF/6-31+G(d,p) level, respectively. The presence of diffuse functions is necessary in evaluating the solvation energy of charged species. The basicity investigations were carried out using the Gaussian 98 program.¹⁸

Results and Discussion

Photoelectron Spectra and Energy Levels. In the case of 1-phenylphosphole (**3**),²⁸ the photoelectron spectrum shows two bands of equal intensity at 8.45 and 9.25 eV. First, we will try to assign these two bands which are related to *vertical ionization energies*. Subsequently, the splitting of the first two ionization energies of the parent phosphole (**1**) and substituted phospholes (**2–9**) (Figure 1) will be discussed. Finally, we will consider *adiabatic ionization energies* and find out what sort of electron is most easily removed in these 1H-phospholes.

In the study of the electronic structure of phospholes, an understanding of the π -system is of basic importance. As illustrated in Figure 2, the phosphole π -system can be built up from the π -MOs of a *cis*-1,3-butadiene unit and the HOMO of a phosphine unit that carries electron density in the region of the P–H bonds and the phosphorus lone pair. The *cis*-1,3-butadiene HOMO has a nodal plane containing the P atom and thus remains unperturbed as the phosphole HOMO (8a'') is formed. The *cis*-1,3-butadiene HOMO-1 shows a bonding and an antibonding interaction with the HOMO of phosphine, resulting in the HOMO-2 (13a') and HOMO-1 (14a') of phosphole, respectively.

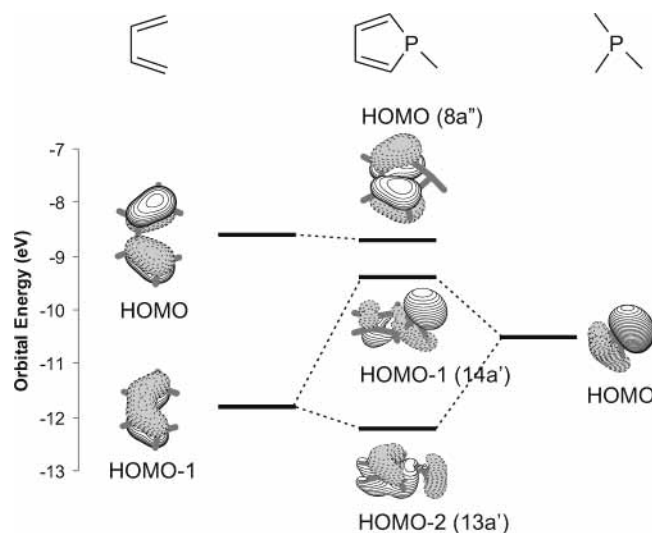


Figure 2. Orbital interaction diagram describing the formation of the valence electronic structure of phosphole. The π orbitals of *cis*-1,3-butadiene are shown on the left, the HOMO of phosphine on the right, and the resulting molecular orbitals of phosphole are in the center.

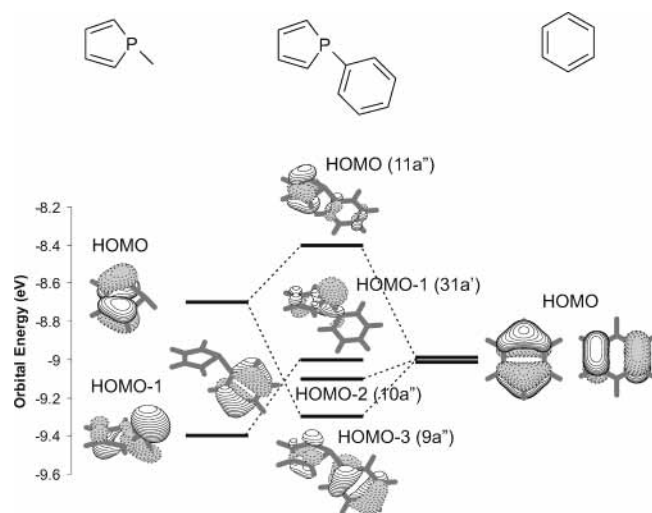


Figure 3. Orbital interaction diagram describing the formation of the valence electronic structure of 1-phenylphosphole. The π -orbitals of phosphole are shown on the left, the degenerate HOMO of phenyl on the right, and the resulting molecular orbitals are in the center.

Furthermore, when substituents are added, we need to consider the interactions between the phosphole and substituent orbitals whereby the possibility of an interaction is determined by the energy and symmetry of the concerned orbitals. Let us take 1-phenylphosphole (**3**) as an example. Figure 3 shows that the highest occupied MOs of 1-phenylphosphole can be constructed from the HOMO and HOMO-1 of the phosphole moiety and the degenerate HOMO of benzene. The HOMO of phosphole interacts in a bonding and an antibonding way with the HOMO of benzene, forming the HOMO-3 (9a'') and HOMO (11a'') of 1-phenylphosphole at -9.3 and -8.4 eV, respectively, according to HF/6-31G* calculations. The interaction between the HOMO-1 of phosphole and the HOMO of benzene is not symmetry allowed. As a consequence, the HOMO-1 (31a') of 1-phenylphosphole at -9.0 eV is almost the HOMO-1 of phosphole, whereas the HOMO-2 (10a'') at -9.1 eV corresponds to the HOMO of benzene.

As mentioned above, the photoelectron spectrum of 1-phenylphosphole²⁸ shows two bands of equal intensity centered at 8.45 and 9.25 eV. According to Schäfer et al.,²⁸ the intensity

TABLE 1: Splitting between the First Two Ionization Energies (eV) of the Phospholes Considered^a

	IE(1)		IE(2)		DIE	
	calcd	expt ^b	calcd	expt ^b	calcd	expt ^b
1	8.7		9.4		0.7	
2	8.5		8.9		0.4	
3	8.4	8.45	9.0	8.45	0.6	0.00
4	7.9	8.00	9.0	8.50	1.1	0.50
5	8.2		8.8		0.6	
6	8.4		9.1		0.7	
7	9.1		9.8		0.7	
8	8.3		8.7		0.4	
9	8.1		8.3		0.2	

^a Phosphole (1), 1-methylphosphole (2), 1-phenylphosphole (3), 2,5-dimethyl-1-phenylphosphole (4), 3,4-dimethyl-1-phenylphosphole (5), 3,4-dimethylphosphole (6), 3,4-dimethyl-1-cyanophosphole (7), 3,4-dimethyl-1-isopropoxyphosphole (8), and 3,4-dimethyl-1-dimethylaminophosphole (9). ^b Reference 28.

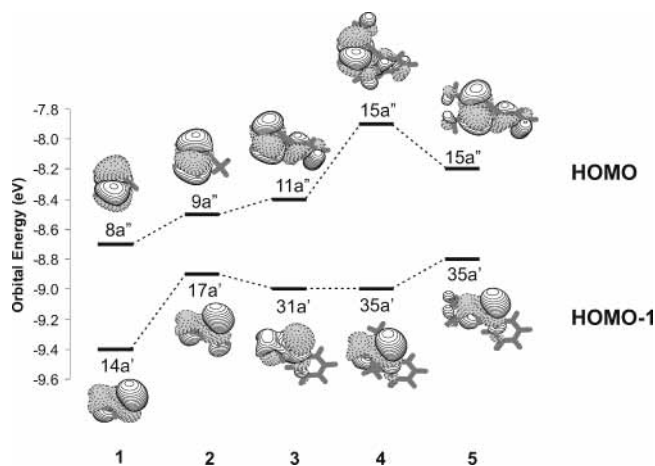


Figure 4. Orbital correlation diagram of the two highest π MOs of phosphole (1), 1-methylphosphole (2), 1-phenylphosphole (3), 2,5-dimethyl-1-phenylphosphole (4), and 3,4-dimethyl-1-phenylphosphole (5).

and the shape of the first band indicate that there must be two distinct ionizations in this region, that were assigned to the removal of an electron from the HOMO of *cis*-1,3-butadiene and the lone pair of phosphine, respectively. The second band was related to an ionization from the HOMO of benzene. These earlier investigations thus led to the assumption that the P lone pair takes no part in a five-membered cyclic conjugation. By using the orbital energies, it seems possible to assign the first band to the ionization of the HOMO (11a'') of phosphole which amounts to -8.4 eV, whereas the energy of HOMO-1 (31a'') at -9.0 eV is computed on the lower side of experiment. If the HOMO-1 participates in the first band, as suggested by Schäfer et al.,²⁸ then the second band could be assigned to electron rejection form HOMO-2 (10a'') whose energy is at -9.1 eV.

In our view, the first two ionization energies of the considered 1*H*-phospholes are likely related to the energies of the HOMO and HOMO-1, respectively. These first two vertical ionization energies, tabulated from orbital energies are recorded in Table 1, and the corresponding orbital correlation diagrams are presented in Figures 4 and 5.

Let us investigate the influence of *P*-methyl and *P*-phenyl substitution on the splitting of the first two ionization energies. In both cases, the HOMO and HOMO-1 orbitals of the parent phosphole (1) are destabilized due to an antibonding interaction between both phosphole and substituent orbitals. In the case of 1-methylphosphole (2), the HOMO-1 is more destabilized than the HOMO, which results in a lowering of the splitting by 0.3

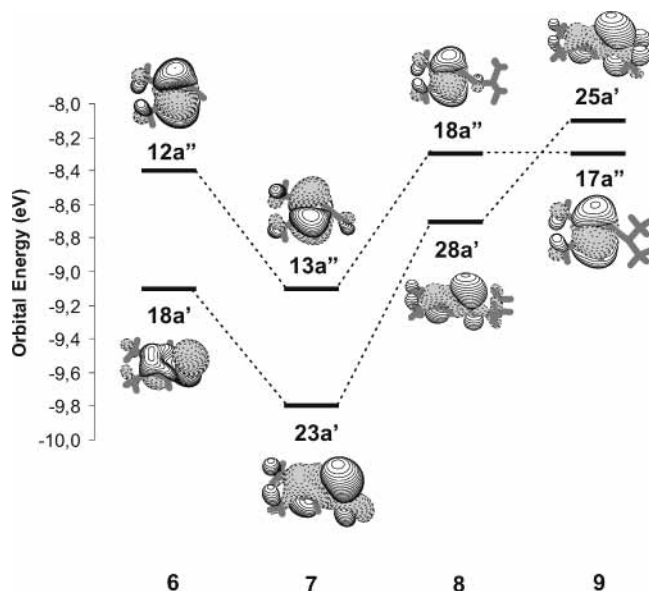
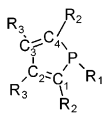


Figure 5. Orbital correlation diagram of the two highest π MOs of 3,4-dimethylphosphole (6), 3,4-dimethyl-1-cyanophosphole (7), 3,4-dimethyl-1-isopropoxyphosphole (8), and 3,4-dimethyl-1-dimethylaminophosphole (9).

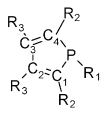
eV. For 1-phenylphosphole (3), we computed that the HOMO and HOMO-1 orbitals are both destabilized about equally. As a consequence, the splitting remains nearly unchanged.

The influence of dimethyl substitution at 2,5- and 3,4-positions of the five-membered ring of 1-phenylphosphole appears to follow a different pattern as compared to 1-phenylphosphole (3). For the 2,5-dimethyl substitution (4), a strong antibonding interaction is observed between the methyl pseudo π -orbitals and the HOMO of 1-phenylphosphole, whereas no interactions are symmetry allowed with the HOMO-1. This results in an increase of the splitting by up to 0.5 eV. This is in excellent agreement with the measured value of 0.5 eV for (4) reported by Schäfer et al.²⁸ Furthermore, in the case of 3,4-dimethyl substitution, the methyl pseudo π -orbitals interact in an antibonding way with both HOMO and HOMO-1 orbitals of 1-phenylphosphole. Consequently, they remain parallel and there is no appreciable change of the splitting. We also notice that the interaction between the methyl pseudo π -orbitals and the HOMO of 1-phenylphosphole is less pronounced at the 3,4- as compared to the 2,5-positions.

Finally, we considered the influence of π -acceptor and π -donor groups such as cyano and isopropoxy, dimethylamino, respectively, at the P position of 3,4-dimethylphosphole (5). The resulting 3,4-dimethyl-1-cyano- (7), 3,4-dimethyl-1-isopropoxy- (8), and 3,4-dimethyl-1-dimethylaminophosphole (9) were compared to 3,4-dimethylphosphole (6). For the *P*-cyano substitution, we computed that the HOMO and HOMO-1 orbitals are both strongly stabilized. Nevertheless, due to the parallel downward shift, the splitting does not change. Following *P*-isopropoxy and *P*-dimethylamino substitution, the HOMO of 3,4-dimethylphosphole remains nearly equal, whereas the HOMO-1 gets destabilized by 0.4 and 1.0 eV, respectively. A possible explanation for this substantial destabilization is given by the assumption that the π -donor groups at phosphorus enforce the interaction between the phosphorus lone pair and the *cis*-1,3-butadienic orbital. The result is a lowering of the splitting by 0.3 eV for 3,4-dimethyl-1-isopropoxyphosphole (8) and by 0.5 eV for 3,4-dimethyl-1-dimethylaminophosphole (9). We remark that in the case of *P*-dimethylamino substitution, the HOMO-1 (HOMO) of 3,4-dimethylphosphole (6) interchanges

TABLE 2: Optimized Geometries of Phosphole (1), 1-Methylphosphole (2), 1-Phenylphosphole (3), 2,5-Dimethyl-1-phenylphosphole (4), and 3,4-Dimethyl-1-phenylphosphole (5) and of the Corresponding Most Stable Radical Cations at the B3LYP/6-31G* Level


	Neutral					Radical Cation				
	1	2	3	4	5	1	2	3	4	5
R ₁	H	CH ₃	C ₆ H ₅	C ₆ H ₅	C ₆ H ₅	H	CH ₃	C ₆ H ₅	C ₆ H ₅	C ₆ H ₅
R ₂	H	H	H	CH ₃	H	H	H	H	CH ₃	H
R ₃	H	H	H	H	CH ₃	H	H	H	H	CH ₃
P-C ₁	1.817	1.813	1.815	1.833	1.813	1.813	1.764	1.812	1.823	1.811
C ₁ -C ₂	1.356	1.357	1.356	1.356	1.357	1.411	1.361	1.399	1.412	1.402
C ₂ -C ₃	1.460	1.460	1.461	1.460	1.481	1.402	1.488	1.413	1.399	1.434
∠C ₁ PC ₄	90.3	90.4	90.3	91.2	89.7	87.9	97.8	88.4	89.7	87.3
∠PC ₁ C ₂	109.9	110.0	110.0	108.6	111.2	111.2	105.5	111.2	109.3	112.8
∠C ₁ C ₂ C ₃	114.3	114.2	114.2	115.3	113.3	113.3	115.5	113.4	114.5	112.3
ΣCPX	293.1	300.6	302.5	300.2	300.7	294.5	346.8	297.4	305.3	296.9

TABLE 3: Optimized Geometries of 3,4-Dimethylphosphole (6), 1-Cyano-3,4-dimethylphosphole (7), 1-Isopropoxy-3,4-dimethylphosphole (8), and 3,4-dimethyl-1-dimethylaminophosphole (9) and of the Corresponding Most Stable Radical Cations at the B3LYP/6-31G* Level


	Neutral				Radical Cation			
	6	7	8	9	6	7	8	9
R ₁	H	CN	OCH(CH ₃) ₂	N(CH ₃) ₂	H	CN	OCH(CH ₃) ₂	N(CH ₃) ₂
R ₂	H	H	H	H	H	H	H	H
R ₃	CH ₃	CH ₃	CH ₃	CH ₃	CH ₃	CH ₃	CH ₃	CH ₃
P-C ₁	1.814	1.815	1.814	1.813	1.815	1.825	1.820	1.787
C ₁ -C ₂	1.357	1.354	1.353	1.356	1.409	1.403	1.400	1.356
C ₂ -C ₃	1.479	1.484	1.490	1.484	1.428	1.436	1.437	1.504
∠C ₁ PC ₄	89.7	90.3	90.0	90.0	86.9	89.6	86.3	94.8
∠PC ₁ C ₂	111.1	110.5	110.6	110.7	112.8	112.4	112.1	107.5
∠C ₁ C ₂ C ₃	113.5	113.7	113.4	113.5	112.3	112.5	112.1	114.6
ΣCPX	292.1	295.7	301.6	300.2	291.1	291.7	296.1	320.6

TABLE 4: Adiabatic Ionization Energies (IEs) of Phospholes^a Obtained Using the ΔE Method at the B3LYP/6-31G* Level

structure	neutral			radical cation			IE ^c
	state	E ^b	ZPEC	state	E	ZPEC	
1	¹ A'	-496.74110	0.074 85	² A''	-496.43630	0.074 31	8.3
2	¹ A'	-536.06229	0.104 42	² A'	-535.77140	0.103 29	7.9
3	¹ A'	-727.79646	0.157 91	² A''	-727.51300	0.157 21	7.7
4	¹ A'	-806.43466	0.213 78	² A''	-806.17192	0.212 72	7.1
5	¹ A'	-575.38069	0.131 04	² A''	-575.09339	0.129 69	7.8
6	¹ A'	-806.43591	0.213 75	² A''	-806.16574	0.212 66	7.3
7	¹ A'	-667.62393	0.131 45	² A''	-667.31655	0.129 70	8.3
8	¹ A'	-768.54929	0.221 80	² A''	-768.27755	0.220 46	7.4
9	¹ A'	-709.34430	0.205 66	² A'	-709.10210	0.205 81	6.6

^a Phosphole (1), 1-methylphosphole (2), 1-phenylphosphole (3), 2,5-dimethyl-1-phenylphosphole (4), 3,4-dimethyl-1-phenylphosphole (5), 3,4-dimethylphosphole (6), 1-cyano-3,4-dimethylphosphole (7), 3,4-dimethyl-1-isopropoxyphosphole (8), and 3,4-dimethyl-1-dimethylaminophosphole (9). ^b Energies (E) and zero-point energy corrections (ZPEC) are given in hartrees. ^c Adiabatic ionization energies taking ZPECs into account are given in eV.

becoming the HOMO (HOMO-1) of 3,4-dimethyl-1-dimethylaminophosphole (9) and that the splitting between the first two ionization energies is now reduced to 0.2 eV. The HOMO of 3,4-dimethyl-1-dimethylaminophosphole (9) no longer correlates with the *cis*-1,3-butadiene HOMO. This could explain why, in contrast to 3,4-dimethyl-1-cyanophosphole (7) and 3,4-dimethyl-1-isopropoxyphosphole (8), no cycloaddition with acrylonitrile was observed for 3,4-dimethyl-1-dimethylaminophosphole (9).²⁹

Selected optimized geometrical parameters of the 1*H*-phospholes considered and the corresponding most stable radical

cations are recorded in Tables 2 and 3. The adiabatic ionization energies of these molecules are given in Table 4.

As shown in Tables 2 and 3, it is mainly the *cis*-1,3-butadiene unit which is disturbed when ionizing 1*H*-phospholes, except for 1-methyl- (2) and 3,4-dimethyl-1-dimethylaminophosphole (9). The C₁-C₂ bond lengthens by around 0.05 Å, whereas the central C₂-C₃ bond shortens by a similar value. This indicates that the electron is removed from the HOMO which resembles the *cis*-1,3-butadiene HOMO, possessing π-bonding character between C₁ and C₂ and π-antibonding character between C₂ and C₃. As such, ionization weakens the C₁-C₂ bond when

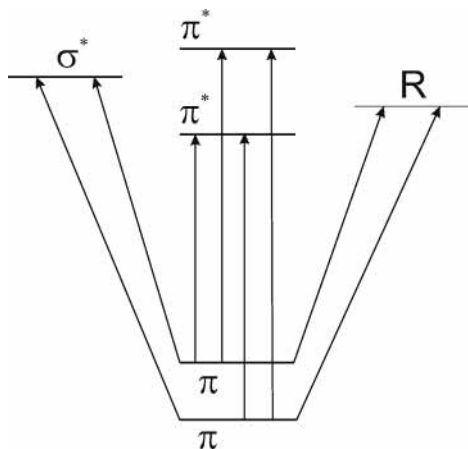


Figure 6. Possible electronic transitions in 1H-phospholes.

going from the neutral to the radical cation. For 1-methyl- (2) and 3,4-dimethyl-1-dimethylaminophosphole (9), it is the C₂–C₃ bond that lengthens by around 0.02–0.03 Å (the other bonds are not changed that much), and the P-unit is flattened considerably in the most stable radical cation as shown by a strong increase of the sum of phosphorus bond angles (Σ CPX). This result points out that the electron is ejected from an orbital which possess π -bonding character between C₂ and C₃ and lone pair character at the P atom as well. For 1-methylphosphole (2), the corresponding HOMO-1 orbital is stabilized through *hyper-conjugation*. The σ -electrons in the neighboring methyl C–H bond also help stabilizing the positive charge. In the case of 3,4-dimethyl-1-dimethylaminophosphole (9), it can be assumed that an electron is removed from the HOMO, which, as mentioned above, corresponds to the HOMO-1 of 3,4-dimethylphosphole (6). As expected, the computed adiabatic ionization energies presented in Table 4 are significantly lower than the vertical ones recorded in Table 1 due to large relaxation of electron and geometry.

In summary, we would conclude that the above investigations demonstrate that a simple MO approach can be useful for giving a qualitative interpretation of not only the PES spectra but also the observed reactivity of the 1H-phospholes considered. A comparison of the structure of the ionic ground state to that of the neutral molecule is necessary to trace the identity of the removed electron.

UV—Vis Electronic Spectra. The understanding of the ground-state electronic structure of phosphole provides us with a solid basis for the investigation of its excited states. Because of the existence of close-lying *valence* and *Rydberg* states, the electronic absorption spectrum of 1H-phospholes is rather complex. Figure 6 shows a manifold of possible electronic transitions including the valence $\pi^* \leftarrow \pi$, $\sigma^* \leftarrow \pi$, and Rydberg transitions. From a technical point of view, the computed energies of the valence states are extremely sensitive to the mixing with Rydberg states. This mixing is reflected in the orbital extension as given by $\langle r^2 \rangle$ (second Cartesian moment). Valence states have an orbital extension similar to that of the ground state. Rydberg states, on the contrary, usually have a more diffuse character. As such, if clear and compact valence states are not observed, then some mixing has likely occurred.

Simple *P*-alkylphospholes possess a unique absorption band, of moderate intensity, in the region 280–290 nm. First noted with 1-methylphosphole³⁰ ($\lambda_{\max} = 286$ nm or $E_{\text{exc}} = 4.3$ eV in isoctane, $f = 0.17$), this band cannot be associated either with the *cis*-1,3-butadiene component of the ring or with the phosphine unit, if considered separately, since neither of the

TABLE 5: Calculated Lowest-lying Valence Excited Singlet States of the Parent Phosphole (1) Using MS-CASPT2 and TD-DFT Methods

state	method	E_{exc}^a	λ^b	f^c	$\langle r^2 \rangle^d$	orbital transition
X ¹ A'	MS-CASPT2 ^e				78	L = LUMO, H = HOMO
	TD-DFT ^f				83	
1 ¹ A''	MS-CASPT2	4.2	294	0.08	83	
	TD-DFT	4.6	268	0.05	88	L(15a') ← H(8a'')
1 ¹ A'	MS-CASPT2	4.8	260	0.23	81	
	TD-DFT	5.0	248	0.11	82	L(15a') ← H-1(14a')

^a The excitation energies are given in eV. ^b The corresponding absorption wavelengths are given in nm. ^c The oscillator strengths. ^d The expectation values for the second Cartesian moments are given in au². ^e MS-CASPT2/ANO-L+diffuse basis functions using MP2/6-311++G(d,p) optimized geometry. ^f TD-DFT/TZVP + diffuse basis functions using MP2/6-311++G(d,p) optimized geometry.

TABLE 6: Lowest Valence Excited Singlet States of the Considered 1H-Phospholes Obtained Using the TD-DFT/B3LYP Method in Conjunction with the SV(P) Basis Set

	state	E_{exc}^a	λ_{\max}^b	f^c	$\langle r^2 \rangle^d$	main contribution
1	X ¹ A'				82	
	1 ¹ A''	4.8	259	0.05	87	HOMO(8a'') → LUMO(15a')
	1 ¹ A'	5.1	245	0.10	80	HOMO-1(14a') → LUMO(15a')
2	X ¹ A'				96	
	1 ¹ A''	4.6	269	0.04	99	HOMO(9a'') → LUMO(18a')
	1 ¹ A'	4.6	267	0.10	97	HOMO-1(17a') → LUMO(18a')
3	X ¹ A'				154	
	1 ¹ A''	4.4	280	0.02	155	HOMO(11a'') → LUMO(32a')
	1 ¹ A'	4.7	265	0.02	154	HOMO(11a'') → LUMO+1(12a')
	2 ¹ A'	4.8	259	0.09	154	HOMO-1(31a') → LUMO(32a')
4	X ¹ A'				183	
	1 ¹ A''	4.3	290	0.07	182	HOMO(15a'') → LUMO(36a')
	2 ¹ A'	4.7	264	0.01	188	HOMO-1(35a') → LUMO(36a')
						HOMO(15a'') → LUMO+2(17a'')
	3 ¹ A'	4.8	256	0.09	188	HOMO-1(35a') → LUMO(36a')
5	X ¹ A'				182	
	1 ¹ A''	4.4	280	0.01	182	HOMO(15a'') → LUMO(36a')
	2 ¹ A'	4.7	261	0.12	185	HOMO-1(35a') → LUMO(36a')
	3 ¹ A'	4.8	256	0.09	188	HOMO(15a'') → LUMO+2(17a'')
						HOMO(15a'') → LUMO(36a')
						HOMO(15a'') → LUMO+2(17a'')
6	X ¹ A'				113	
	1 ¹ A''	4.7	259	0.03	121	HOMO(12a'') → LUMO(19a')
	1 ¹ A'	5.1	245	0.13	105	HOMO-1(18a') → LUMO(19a')
7	X ¹ A'				147	
	1 ¹ A''	4.6	270	0.02	151	HOMO(13a'') → LUMO(24a')
	1 ¹ A'	4.9	255	0.08	134	HOMO-1(23a') → LUMO(24a')
8	X ¹ A'				160	
	1 ¹ A''	4.0	309	0.01	161	HOMO(18a'') → LUMO(29a')
	1 ¹ A'	4.1	301	0.13	164	HOMO-1(28a') → LUMO(29a')
9	X ¹ A'				150	
	1 ¹ A'	3.3	380	0.06	145	HOMO(25a') → LUMO(26a')
	1 ¹ A''	4.3	288	0.02	153	HOMO-1(17a'') → LUMO(26a')

^a The excitation energies are given in eV. ^b The corresponding absorption wavelengths are given in nm. ^c The oscillator strengths. ^d The expectation values for the second Cartesian moments are given in au².

two moieties have typical absorption bands near this region. Hence, this band seems to be clearly descriptive for the phosphole ring system. In this context, it is of importance to investigate the electronic origin of the observed band and the effect of substituents on its location in the absorption spectrum. A comparison between the lowest valence excited states of the parent phosphole (1) obtained with both the MS-CASPT2 and TD-DFT methods, is given in Table 5. Table 6 describes the lowest valence excited singlet states obtained for all 1H-phospholes considered using the TD-DFT method.

Table 5 points out that the lowest excited ¹A'' and ¹A' states of the parent phosphole (1) are of single-reference character

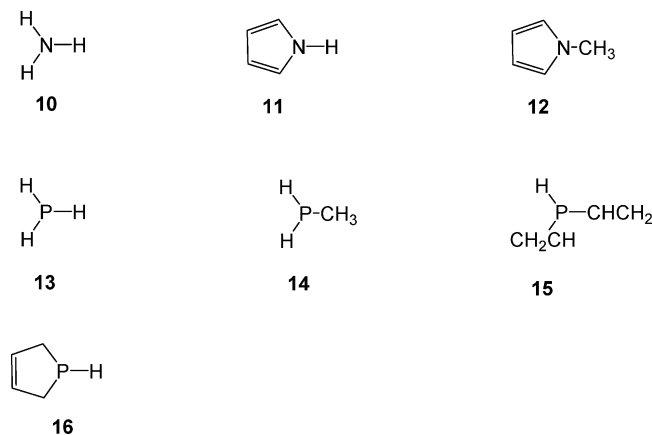


Figure 7. Structure of ammonia (**10**), pyrrole (**11**), 1-methylpyrrole (**12**), phosphine (**13**), 1-methylphosphine (**14**), divinylphosphine (**15**), and phospholene (**16**).

and related to $\pi^* \leftarrow \pi$ transitions. They are dominated by the LUMO(15a') \leftarrow HOMO(8a'') and LUMO(15a') \leftarrow HOMO-1(14a') transitions, respectively. The $\langle r^2 \rangle$ values show that the lowest $\pi^* \leftarrow \pi$ transitions do not mix with Rydberg states. The vertical excitation energy leading to the $1^1A''$ state is computed in gas phase to be 4.2 eV with a weak oscillator strength of $f = 0.08$ at the MS-CASPT2 level, whereas the excitation energy for the $1^1A'$ state is calculated at 4.8 eV, with a stronger oscillator strength of $f = 0.23$. Since the experimental spectrum exhibits only one band, we could assume that both closely lying transitions may be overlapped in the experimental band.

Furthermore, Table 5 shows that the TD-DFT method computes the valence excitation energies systematically higher and the oscillator strengths systematically lower than those derived using the MS-CASPT2 method, whereas the expectation values for $\langle r^2 \rangle$ are similar. The difference between the TD-DFT and MS-CASPT2 values is consistent and amounts up to 0.4 eV. From this comparison, it can be concluded that the TD-DFT approach yields results that are qualitatively comparable to those obtained with the MS-CASPT2 method but quantitatively less accurate.

TABLE 7: Computed PA's (kJ/mol) at Different Sites in Gas Phase of the 1*H*-Phospholes 1–9 and Structures 10–16^a

	N/P	C _α	C _β	expt ^b
1	844.1	844.5	797.4	
2	896.9	873.0	852.4	
3	909.9	889.8	871.3	
4	933.9	913.2	894.7	
5	950.1	932.4	882.2	
6	885.7	892.0	870.8	
7	823.0	840.9	741.7	
8	950.2	934.4	869.5	
9	965.9	964.4	903.2	
10	854.0			853.5
11	789.6	878.0	854.6	875.3
12	811.7	903.6	886.5	
13	783.9			786.6
14	852.6			851.4
15	930.5	869.5	870.2	
16	890.7	760.9		

^a PA values computed at B3LYP/6-311++G(d,p)//HF/6-31G(d,p) level. ^b Reference 35.

In view of the systematic deviation, it seems reasonable to use the more economical TD-DFT method to predict the shifting of the lowest excited $1^1A''$ and $1^1A'$ states along the series of substituted phosphole rings. Table 6 reveals that substitution of a methyl or phenyl group at the P atom of the parent phosphole (**1**) red-shifts the $1^1A''$ state by 10 and 21 nm, respectively, whereas, the $1^1A'$ state is red-shifted by 22 and 14 nm, respectively. We also notice that in the case of 1-phenylphosphole (**3**), the lowest $1^1A'$ states are described by two electronic configurations. Dimethyl substitution at 2,5-position of the 1-phenylphosphole ring causes a red-shift of the $1^1A''$ state of (**3**) by 10 nm, whereas the absorption wavelengths of the lowest $1^1A'$ transitions remain nearly unchanged. In the case of dimethyl substitution at 3,4-position (**5**), neither of the low-lying $\pi^* \leftarrow \pi$ transitions are seriously shifted.³¹ The $1^1A''$ and $1^1A'$ states of 3,4-dimethylphosphole (**6**) are predicted to red-shift by around 10 nm when putting a cyano group (**7**) at the P atom. For 3,4-dimethyl-1-isopropoxyphosphole (**8**), we found that these states are red-shifted by around 50–55 nm as compared to 3,4-dimethylphosphole (**6**). Finally, we computed

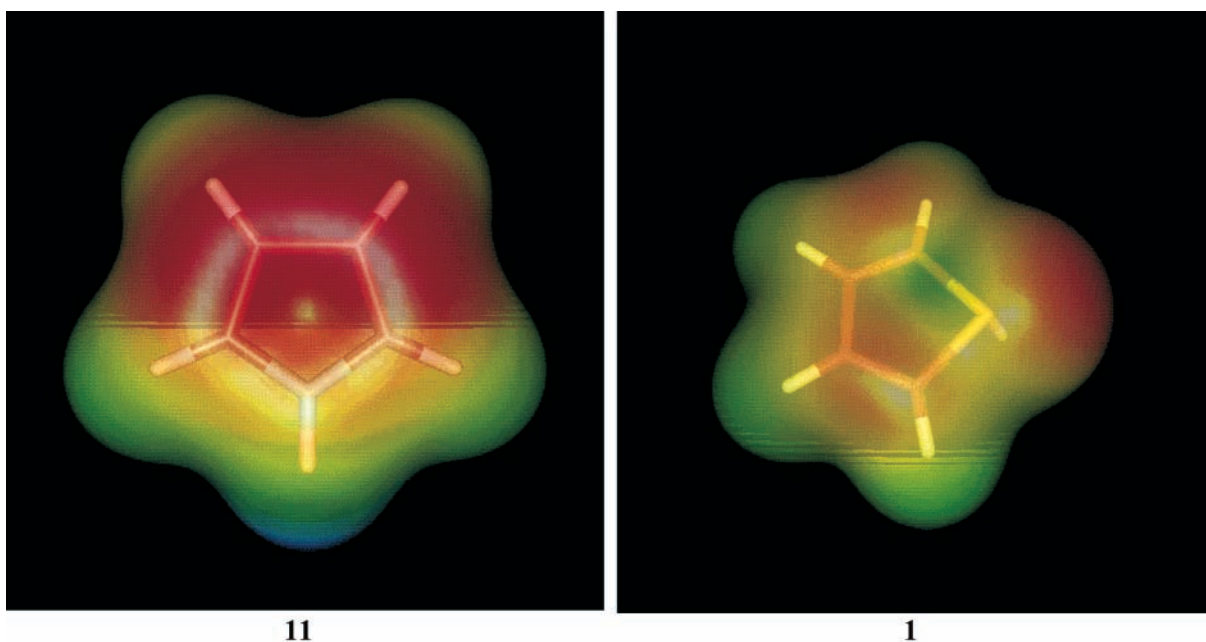


Figure 8. Calculated electron density in pyrrole (**11**) and parent phosphole (**1**). The picture shows the surface where the electron density is 0.002 electrons/Å³. The color code shows the electrostatic potential at this surface, reddish portions representing negative potential.

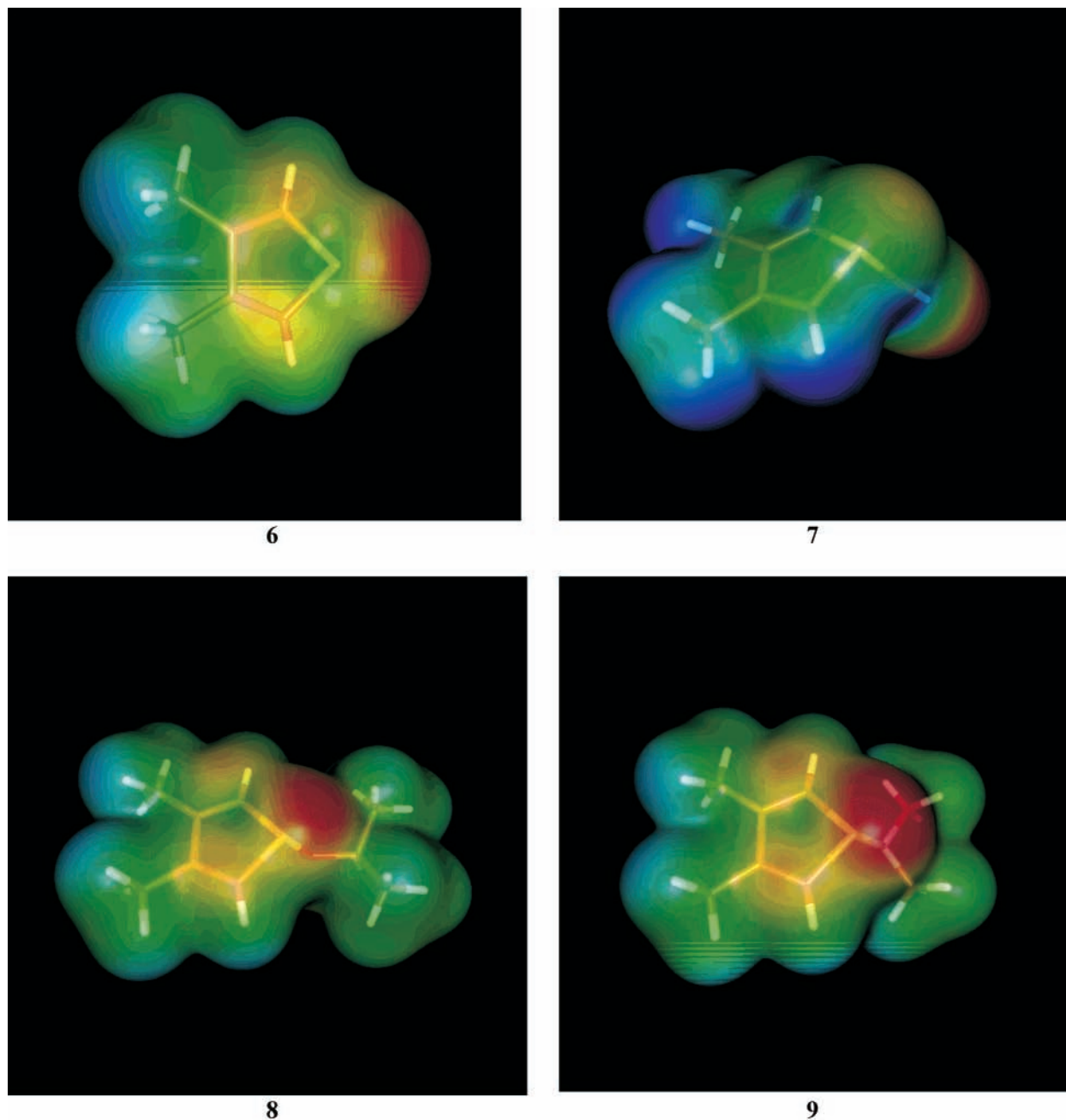


Figure 9. Calculated electron density in 3,4-dimethylphosphole (**6**), 1-cyano-3,4-dimethylphosphole (**7**), 3,4-dimethyl-1-isopropoxyphosphole (**8**), and 3,4-dimethyl-1-dimethylaminophosphole (**9**). The picture shows the surface where the electron density is 0.002 electrons/Å³. The color code shows the electrostatic potential at this surface, reddish portions representing negative potential.

the $1^1A'$ and $1^1A''$ absorption wavelengths for 3,4-dimethyl-1-dimethylaminophosphole (**9**) at 380 and 288 nm, respectively. As a consequence, we expect a very large red-shift of the $1^1A'$ state ($\Delta\lambda_{\text{max}} = 135$ nm) when substituting H by a dimethylamino group at the P atom of 3,4-dimethylphosphole (from **6** to **9**).

Basicity. A remarkable property of 1*H*-phospholes is the observed reduced *basicity* relative to phospholenes and divinylphosphines.^{2,3} We have thus attempted to find out the reasons for such low basicity by a simple comparison of geometric and electronic structures. Furthermore, it has been suggested that phospholes undergo protonation at the P atom,³² whereas in pyrroles, the C_α atom^{2,3} is actually preferred. To check further this information, the *site of protonation* in these systems has been reexamined. Besides this, the effects of substituents on the basicity of phospholes have been investigated

in a systematic way. All structure–property relationships have been analyzed both in *gas phase* and in *acidic solution*.

The molecules selected for the PA and p*K*_a calculations include ammonia (**10**), pyrrole (**11**), 1-methylpyrrole (**12**), phosphine (**13**), 1-methylphosphine (**14**), divinylphosphine (**15**), phospholene (**16**), and the 1*H*-phospholes (**1–9**). These structures are presented in Figure 7 and Figure 1, respectively.

The computed PA values at different protonation sites in the *gas phase* are given in Table 7 for the 1*H*-phospholes **1–9** and for structures **10–16** along with experimental data. We notice that the computed PA values deviate from the available experimental ones by at most 3 kJ/mol. The results are organized as follows: first, we will discuss the sites of protonation of the aforementioned molecules. Subsequently, the basicity of phosphole (**1**), divinylphosphine (**15**), and phospholene (**16**) will be

TABLE 8: Internal \angle CPC Bond Angles (deg) of Neutral and Protonated Forms of Divinylphosphine (15), Phospholene (16), and Parent Phosphole (1) and the Deviation from the Tetrahedral Angle for the Protonated Structures

	\angle CPC	\angle CPC _{H+}	$\Delta_{109.5^\circ} \angle$ CPC _{H+}
1	90.2	95.5	14.0
15	100.9	115.6	6.1
16	91.6	98.9	10.6

compared. Finally, we will comment on the basicity of the substituted 1*H*-phospholes.

Site of Protonation. The results tabulated in Table 7 indeed confirm that that for pyrrole (**11**) and 1-methylpyrrole (**12**), protonation takes place at the C_α atom, whereas for divinylphosphine (**15**), phospholene (**16**), and 1-methylphosphole (**2**), the P atom protonation is favored. For phosphole (**1**), the PA values at both P and C_α sites are nearly identical. In view of their geometry, consideration of the corresponding π -systems may help us to understand the above results. Pyrrole is an aromatic five-membered ring in which the nitrogen lone pair is strongly delocalized toward the *cis*-1,3-butadiene unit. On the contrary, pyramidal phosphole is nonaromatic, since the phosphorus lone pair is only weakly delocalized toward the *cis*-1,3-butadiene unit. As a consequence, we expect on one hand that the nitrogen lone pair is less available for proton bonding than the phosphorus lone pair. On the other hand, the carbon atoms of pyrrole become more electron-rich than those of phosphole and therefore more basic. These findings are visualized in Figure 8 which illustrates the computed electron densities and molecular electrostatic potentials in pyrrole and phosphole.

The PA values recorded in Table 7 reveal that for 3,4-dimethylphosphole (**6**) and 1-cyano-3,4-dimethylphosphole (**7**), protonation now preferentially occurs at C_α, whereas for 1-phenylphosphole (**3**), 2,5-dimethyl-1-phenylphosphole (**4**), 3,4-dimethyl-1-phenylphosphole (**5**), and 3,4-dimethyl-1-isopropoxyphosphole (**8**), the P atom remains the most basic site. For 3,4-dimethyl-1-dimethylaminophosphole (**9**), the PA values at both P and C_α sites are computed to be almost equal. To predict in a qualitative way the site of protonation in substituted phospholes, the molecular electrostatic potential (MEP) can be plotted on an isodensity surface. Comparison of the MEP plot of phosphole (**1**) in Figure 8 with the MEP plot of 3,4-dimethylphosphole (**6**) in Figure 9, reveals that the MEP at C_α becomes more negative when putting methyl groups at 3,4-position of the phosphole ring, and supports the assumption that for 3,4-dimethylphosphole protonation will take place at C_α. Figure 9 also clearly illustrates the influence of π -acceptor or π -donor groups at the P atom of 1*H*-phospholes. As could be expected, the cyano group withdraws electron density from the phosphorus lone pair. As a result, the MEP at phosphorus becomes more positive, and the probability of protonation at the P atom is weakened. As also shown in Figure 9, the reverse trend holds true for π -donor groups such as isopropoxy and dimethylamino.

Basicity. The following ordering is obtained when comparing the gas phase P atom PA's of phosphole (**1**), divinylphosphine (**15**), and phospholene (**16**): PA (phosphole) < PA (phospholene) < PA (divinylphosphine). Table 8 points out that the deviation of the internal bond angle of the quaternary protonated form (\angle CPC_{H+}) from the ideal tetrahedral bond angle (109.5°) is largest in phosphole (**1**) and smallest in divinylphosphine (**15**). Therefore, we expect that the difficulty encountered for protonation is the largest in phosphole and the smallest in divinylphosphine, which could in part explain the reduced

TABLE 9: Computed and Experimental p*K*_a Values at Different Protonation Sites in Acidic Solution of 1*H*-Phospholes 1–9 and Structures 10–16

	N/P	C _α	C _β	expt
1	−5.3	−8.3	−18.1	
2	−0.3	−4.8	−7.3	0.5 ^b
3	2.0	−5.1	−11.5	
4	0.8	−5.3	−9.7	
5	4.6	−1.0	−11.7	
6	−0.6	−3.5	−18.8	
7	−4.9	−9.6	−30.7	
8	−1.2	−1.1	−14.3	
9	2.2			
10	9.2			9.3 ^a
11	−13.8	1.0	−4.0	0 ^a
12	−13.3	1.2	−2.1	
13	−2.0			
14	0.7			
15	4.7			5.2 ^b
16	3.2			

^a Reference 36. ^b Reference 30.

basicity of phospholes as compared to phospholene and divinylphosphine. The above explanation is similar to the suggestion^{33,34} that one of the likely causes of the reduced nucleophilicity of 1,2,5-triphenylphospholes, as compared to triphenylphosphines, is the inherent increase in ring strain of the five-membered phosphole ring upon conversion from a trivalent into a quaternary coordination state. However, in the gas phase, parent phosphole (**1**) is more basic than parent phosphine (**13**) thanks to a stabilization of the positive charge through the *cis*-1,3-butadiene unit.

Furthermore, the results in Table 7 indicate that alkyl-, aryl-, and π -donor groups tend to increase the basicity of 1*H*-phospholes, whereas π -acceptor groups such as cyano weaken it. The increase in basicity is calculated to be strongest in the case of *P*-dimethylamino substitution.

The computed and experimental p*K*_a values at different protonation sites of the 1*H*-phospholes (**1–9**) and structures **10–16** in acidic solution are recorded in Table 9. We notice that the computed and experimental values are in reasonable agreement with each other with deviation of less than one p*K*_a unit. The results also show that for all the molecules considered, the preferred *protonation site* in acidic solution remains the same as in gas phase, except for phosphole (**1**), 3,4-dimethylphosphole (**6**), and 1-cyano-3,4-dimethylphosphole (**7**), where the P atom becomes more basic than the C_α atom. We also see that the *relative basicity* between phosphole, phospholene, and divinylphosphine is not changed in going from the gas phase to acidic solution. However, in a few cases, the relative ordering is modified. Relative to PH₃ (**13**), the parent phosphole (**1**) becomes substantially less basic in acidic solution, which is in contrast to the PA ordering found in the gas phase. Thus, the most marked result here is a reversed basicity ordering between PH₃ and phosphole following solvation. As far as we know, there is actually no reliable experimental value for the p*K*_a of PH₃. It can however be admitted that the PH₄⁺ cation is more stabilized in solution due to the presence of four H atoms that give rise to additional H bonds. It appears that H bonds in the protonated form of PH₃ modify the basicity ordering between PH₃ and phosphole. It is apparent that the basicity of phosphines could be changed upon solvation, and this problem needs to be investigated in detail in future studies. Furthermore, the p*K*_a values indicate that *P*-alkoxy and *P*-amino phosphole derivatives, bearing strong electron donors, become significantly more basic than the parent phospholes.

Concluding Remarks

In summary, the above theoretical investigations demonstrate that a simple MO approach can already be useful for giving a qualitative interpretation of not only the PES spectra but also of the observed reactivity of the 1H-phospholes considered. A comparison of the structure of the ionic ground state to that of the neutral molecule is necessary to trace the identity of the removed electron. We were also able to assign the typical absorption band of P-alkylphospholes to the lowest excited $1^1A''$ and $1^1A'$ states, whose dominant transitions originate from the HOMO and HOMO-1, respectively. The effect of substituents on the related $\pi^* \leftarrow \pi$ transitions could be clearly described. Thereby striking is the very large red-shift ($\Delta\lambda_{\max} = 135$ nm) of the $1^1A'$ state when substituting H by a dimethylamino group at the P atom of 3,4-dimethylphosphole. As what concerns the basicity, our computations support the idea that one of the likely causes of the reduced basicity of phospholes, as compared to phospholenes and divinylphosphines, is the inherent increase in ring strain of the five-membered phosphole ring upon conversion from the trivalent into the quaternary coordination state. There is a reversed ordering of basicity between the parent phosphole (**1**) and the parent phosphine (**13**) in going from the gas phase to acidic solution.

Acknowledgment. The authors thank the FWO-Vlaanderen, the Flemish government, and the KULeuven Research Council (Concerted Research Action, GOA-program) for continuing support.

References and Notes

- Mathey, F. *Chem. Rev.* **1988**, *88*, 429.
- Hughes, A. N. In *Handbook of Organophosphorus Chemistry*; Engel, R., Ed.; Marcel Dekker: New York, 1992; p 483.
- Quin, L. D. *Compr. Heterocycl. Chem.* **1996**, *2*, 757.
- Quin, L. D. Phospholes. In *Phosphorus-Carbon Heterocyclic Chemistry: The Rise of a New Domain*; Mathey, F., Ed.; Elsevier: Oxford, England, 2001; p 219.
- Mathey, F. Phospholes. In *Science of Synthesis*; Maas, G., Ed.; Thieme: Stuttgart, Germany, 2001; p 553.
- Szabo, A.; Ostlund, N. *Modern Quantum Chemistry: Introduction to advanced electronic structure theory*; Dover Publications: New York, 1996.
- Nyulászai, L.; Veszprémi, T. *Int. J. Quantum Chem.* **1997**, *61*, 399.
- Anderson, K.; Malmqvist, P. Å.; Roos, B. O. *J. Chem. Phys.* **1992**, *96*, 1218.
- Finley, J.; Malmqvist, P. Å.; Roos, B. O.; Serrano-Andrés, L. *Chem. Phys. Lett.* **1998**, *288*, 299.
- Casida, M. E. In *Recent advances in density functional methods—Part I*; Chong, D. P., Ed.; World Scientific: Singapore, 1995; p 155.
- Bauernschmitt, R.; Ahlrichs, R. *Chem. Phys. Lett.* **1996**, *256*, 454.
- Almlöf, J.; Taylor, P. R. *J. Chem. Phys.* **1987**, *86*, 4070.
- Widmark, P.-O.; Malmqvist, P.-Å.; Roos, B. O. *Theor. Chim. Acta* **1990**, *77*, 291.
- Dunning, T. H.; Hay, P. J. In *Methods of electron structure theory*; Schaefer, H. F., III, Ed.; Plenum: New York, 1977.
- Kaufmann, K.; Baumeister, W.; Jungen, M. *J. Phys. B: At., Mol., Opt. Phys.* **1989**, *22*, 2223.
- Schäfer, A.; Huber, C.; Ahlrichs, R. *J. Chem. Phys.* **1994**, *100*, 5829.
- Polly, R.; Taylor, P. R. *J. Phys. Chem. A* **1999**, *103*, 10343.
- Frisch, M. J.; Trucks, G. W.; Schlegel, H. B.; Scuseria, G. E.; Robb, M. A.; Cheeseman, J. R.; Zakrzewski, V. G.; Montgomery, J. A.; Stratmann, R. E., Jr.; Burant, J. C.; Dapprich, S.; Millam, J. M.; Daniels, A. D.; Kudin, K. N.; Strain, M. C.; Farkas, O.; Tomasi, J.; Barone, V.; Cossi, M.; Cammi, R.; Mennucci, B.; Pomelli, C.; Adamo, C.; Clifford, S.; Ochterski, J.; Petersson, G. A.; Ayala, P. Y.; Cui, Q.; Morokuma, K.; Malick, D. K.; Rabuck, A. D.; Raghavachari, K.; Foresman, J. B.; Cioslowski, J.; Ortiz, J. V.; Stefanov, B. B.; Liu, G.; Liashenko, A.; Piskorz, P.; Komaromi, I.; Gomperts, R.; Martin, R. L.; Fox, D. J.; Keith, T.; Al-Laham, M. A.; Peng, A. Nanayakkara, C. Y.; Gonzalez, C.; Challacombe, M.; Gill, P. M. W.; Johnson, B.; Chen, W.; Wong, M. W.; Andres, J. L.; Gonzalez, C.; Head-Gordon, M.; Replogle, E. S.; Pople, J. A. *GAUSSIAN 98*, Revision A.5. Gaussian Inc., Pittsburgh, PA, 1998.
- Andersson, K.; Barysz, M.; Bernhardsson, A.; Blomberg, M. R. A.; Carissan, Y.; Cooper, D. L.; Cossi, M.; Fleig, T.; Fülischer, M. P.; Gagliardi, L.; de Graaf, C.; Hess, B. A.; Karlström, G.; Lindh, R.; Malmqvist, P.-Å.; Neogrády, P.; Olsen, J.; Roos, B. O.; Schimmelpfennig, B.; Schütz, M.; Seijo, L.; Serrano-Andrés, L.; Siegbahn, P. E. M.; Stålring, J.; Thorsteinsson, T.; Veryazov, V.; Wierzbowska, M.; Widmark, P.-O. *MOLCAS*, Version 5.2. Lund University, Lund, Sweden, 2001.
- Ahlrichs, R.; Bär, M.; Baron, H.-P.; Bauernschmitt, R.; Böcker, S.; Ehrig, M.; Eichkorn, K.; Elliott, S.; Furche, F.; Haase, F.; Häser, M.; Horn, H.; Hättig, C.; Huber, C.; Huniar, U.; Kattannek, M.; Köhn, A.; Kölmel, C.; Kollwitz, M.; May, K.; Ochsenfeld, C.; Öhm, H.; Schäfer, A.; Schneider, U.; Treutler, O.; von Arnim, M.; Weigend, F.; Weis, P.; Weiss, H. *TURBOMOLE*, Version 5.0, University of Karlsruhe, Karlsruhe, Germany, 1998.
- Ann, M. S.; Igor, A. T.; Christopher, J. M.; *Theor. Chim. Acta* **1995**, *92*, 83.
- Zvonimir, B. M.; Borisslav, K.; Damir, K. *J. Phys. Chem. A* **1997**, *101*, 7446.
- Topol, I. A. Tawa, G. J.; Burt, S. K. *J. Phys. Chem. A* **1997**, *101*, 10075.
- Yevgeniy, P.; Leonid, G.; Jerzy, L. *J. Phys. Chem. A* **2000**, *104*, 7346.
- Matthew, D. L.; George, C. S. *J. Am. Chem. Soc.* **2001**, *123*, 7314.
- Jasna, J. K.; Richard, A. F.; Shi-Yi, L.; Wayne, C. G. *Phys. Chem. A* **2002**, *106*, 1327.
- Cossi, M.; Barone, V.; Cammi, R.; Tomasi, J. *Chem. Phys. Lett.* **1996**, *225*, 327.
- Schäfer, W.; Schweig, A.; Märkl, G.; Hauptmann, H.; Mathey, F. *Angew. Chem., Int. Ed. Engl.* **1973**, *12*, 145.
- Mattman, E. 7-phosphanorbonènes: synthèse, coordination et application en catalyse. Ph.D. Thesis, Ecole Polytechnique, Palaiseau, France, 2002.
- Quin, L. D.; Bryson, J. G.; Moreland, C. G. *J. Am. Chem. Soc.* **1969**, *91*, 3308.
- Bruniquel, M.-F.; Labarre, J.-F.; Mathey, F. *Phosphorus* **1974**, *3*, 269.
- Quin, L. D.; Belmont, S. E.; Mathey, F. *J. Chem. Soc., Perkin Trans. 2* **1986**, 629.
- Cadogan, J. I. G.; Scott, R. J.; Gee, R. D.; Gosney, I. *J. Chem. Soc., Perkin Trans. 1* **1974**, 1694.
- Allen, D. W.; Nowell, I. W.; Oades, A. C.; Walker, P. E. *J. Chem. Soc., Perkin Trans. 1* **1978**, 98.
- Hunter, E. P.; Lias, S. G. *J. Phys. Chem. Ref. Data* **1998**, *27*, 3, 413.
- McMurrey, J. In *Handbook of Organic Chemistry*, 3rd ed.; Brooks/Cole: Pacific Grove: CA, 1992.